Inorganic Chemistry

Article

pubs.acs.org/IC

Pyridine Analogues of the Antimetastatic Ru(III) Complex NAMI-A Targeting Non-Covalent Interactions with Albumin

Michael I. Webb, Ryan A. Chard, Yaser M. Al-Jobory, Michael R. Jones, Edwin W. Y. Wong, and Charles J. Walsby*

Department of Chemistry, Simon Fraser University, 8888 University Drive, Burnaby, BC, V5A 1S6, Canada

Supporting Information

ABSTRACT: A series of pyridine-based derivatives of the antimetastatic Ru(III) complex imidazolium [*trans*-$RuCl_4$(1*H*-imidazole)(DMSO-*S*)] (NAMI-A) have been synthesized along with their sodium-ion compensated analogues. These compounds have been characterized by X-ray crystallography, electron paramagnetic resonance (EPR), NMR, and electrochemistry, with the goal of probing their noncovalent interactions with human serum albumin (hsA). EPR studies show that the choice of imidazolium ligands and compensating ions does not strongly influence the rates of ligand exchange processes in aqueous buffer solutions. By contrast, the rate of formation and persistence of interactions of the complexes with hsA is found to be strongly dependent on the properties of the axial ligands. The stability of noncovalent binding is shown to correlate with the anticipated ability of the various pyridine ligands to interact with the hydrophobic binding domains of hsA. These interactions prevent the oligomerization of the complexes in solution and limit the rate of covalent binding to albumin amino acid side chains. Electrochemical studies demonstrate relatively high reduction potentials for these complexes, leading to the formation of Ru(II) species in aqueous solutions containing biological reducing agents, such as ascorbate. However, EPR measurements indicate that while noncovalent interactions with hsA do not prevent reduction, covalent binding produces persistent mononuclear Ru(III) species under these conditions.

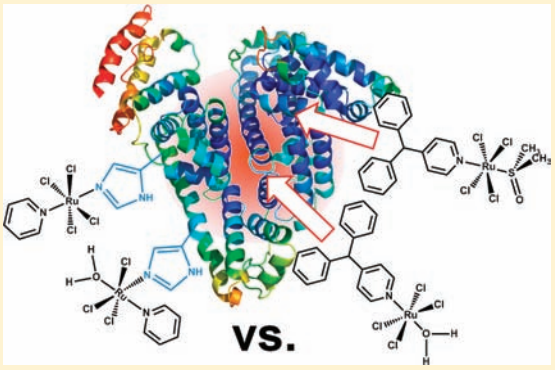

INTRODUCTION

Ru(III) complexes have recently drawn increasing attention as the next generation of metal-based alternatives to platinum-based anticancer drugs.[1−3] Not only do many of these compounds exhibit potent cytotoxic or antimetastatic activity, but they are frequently found to have low levels of side effects. Two of these complexes, imidazolium [*trans*-$RuCl_4$(1*H*-imidazole)(DMSO-*S*)] (NAMI-A) and indazolium [*trans*-$RuCl_4$(1*H*-indazole)$_2$] (KP1019) (Figure 1), have completed phase-I clinical trials successfully and are now undergoing further clinical investigations.[4−6]

The Ru(III) anticancer compounds with proven clinical activity are generally negatively charged octahedral complexes containing axial heterocyclic nitrogen donor ligands and equatorial chlorides, with charge compensation provided by protonated nitrogen heterocycles or sodium ions. NAMI-A and related complexes, with a single axial heterocyclic nitrogen ligand and dimethylsulfoxide (DMSO) at the other axial position, were first described by Sava and co-workers,[7,8] and have been intensively studied. Despite modest cytotoxic activity, these complexes have attracted significant interest because of their ability to prevent the formation of metastases and inhibit their growth.[9,10] The other major family of active Ru(III) compounds are bis-azole complexes such as KP1019 and imidazolium [*trans*-$RuCl_4$(1*H*-imidazole)$_2$] (KP418) (Figure 1), which were initially characterized by Keppler and co-workers in the early 1990s.[11−13] These "Keppler-type" complexes generally show more conventional antineoplastic properties.[1,3,5] It is now widely accepted that both types of compounds are prodrugs, which are activated in vivo by processes that are modulated by their axial ligands.[1,3,14] A variety of studies have demonstrated that complicated ligand exchange processes occur when these compounds are dissolved

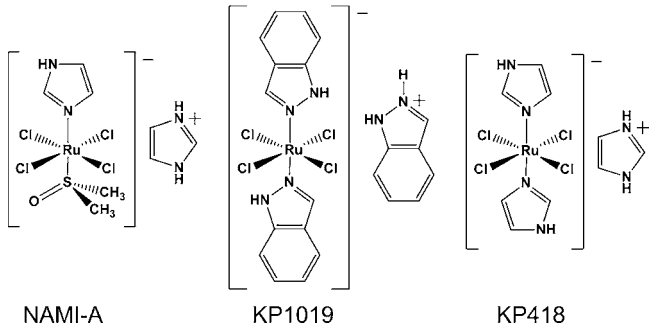

Figure 1. Anticancer Ru(III) complexes.

Received: September 16, 2011
Published: December 23, 2011

in aqueous media, because of the loss of chloride ligands, and DMSO in the case of NAMI-A; the azole ligands are kinetically inert and remain coordinated under physiological conditions.[15] Aquation of NAMI-A occurs readily in buffer solutions to give initially soluble mononuclear Ru(III) products, which are then converted to insoluble oligomers.[15−17] By contrast, aquation of Keppler-type compounds produces solutions of solely mononuclear complexes. In the case of KP1019, this leads to an insoluble monoaqua complex which rapidly precipitates at pH 7.4,[12,18,19] whereas KP418 remains in solution following aquation.[20,21]

Both NAMI-A and Keppler-type Ru(III) anticancer complexes interact readily with serum proteins, particularly human serum albumin (hsA).[17,21−25] Several studies have indicated that these complexes can bind to hsA following ligand exchange, via histidine and cysteine side chains to give relatively stable protein-bound species.[3,5,21] Recently, we have used electron paramagnetic resonance (EPR) spectroscopy to characterize the formation of *noncovalent* interactions of NAMI-A, KP1019, and KP418 with hsA.[17,21] Our studies have demonstrated that the axial heterocyclic ligands play a dominant role, fundamentally influencing the solution behavior of the complexes. A particularly important finding of these studies was that KP1019 forms noncovalent interactions with hsA more readily than KP418.[21] This has been correlated with the greater ability of the indazole ligands of KP1019 to form interactions with the hydrophobic domains of hsA, as compared to the imidazole ligands of KP418. These observations form the basis of our hypothesis that noncovalent interactions with hsA can be tuned to control the speciation and transportation of the complexes in vivo. Specifically, by modifying the heterocyclic axial ligands of NAMI-A derivatives, we have sought to promote binding to the hydrophobic binding sites of hsA. This is a novel drug design strategy which has the potential to accelerate the formation of initial protein interactions, while limiting covalent binding. The latter consideration is particularly important since it impacts on the bioavailability of the compounds.[24,26]

In this work, we have synthesized and structurally characterized a series of NAMI-A analogues with pyridine-based ligands, which were selected for their differing potential to promote noncovalent protein interactions (Figure 2). The

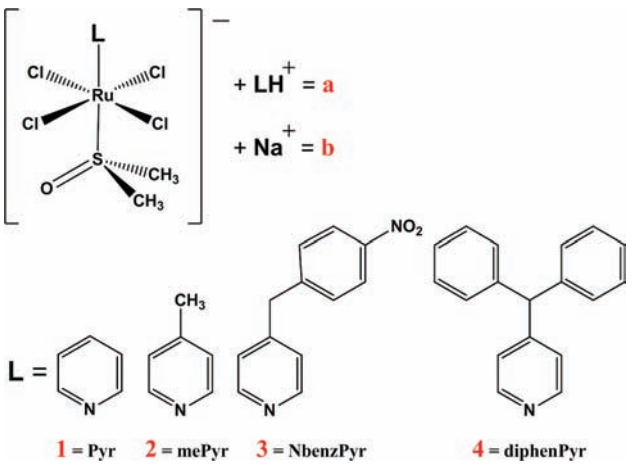

Figure 2. Pyridine analogues of NAMI-A synthesized in this work with four different pyridine-based ligands and two types of counterions.

ligands we have chosen, **1**, pyridine (Pyr); **2**, 4-methylpyridine (mePyr); **3**, 4-(4-nitrobenzyl)pyridine (NbenzPyr); **4**, diphenyl-4-pyridyl-methane (diphenPyr), have the potential to provide steric, hydrophobic, and $\pi-\pi$ stacking interactions with amino acid side chains. In addition to the NAMI-A analogues (series **a**), which have the protonated heterocyclic ligands for counterions, we have also synthesized their sodium-ion compensated counterparts (series **b**), which are analogues of sodium [*trans*-$RuCl_4$(1*H*-imidazole)(DMSO-*S*), also known as NAMI.[27] This has enabled analysis of the effect of the counterions on protein interactions, and has improved the aqueous solubility of the compounds, particularly for the complexes with highly hydrophobic ligands (**3b** and **4b**). The synthesis of complexes with different counterions was also motivated by reports that this has evoked different specificities for the biomolecule interactions and anticancer activity of several Ru(III) complexes.[28]

We have used EPR to characterize the ligand-exchange processes of these compounds and their interactions with hsA. These studies demonstrate that the aqueous solution behavior of the complexes is similar to NAMI-A, with exchange of Cl^- and DMSO ligands. However, the pyridine ligands have significant and distinct effects on the interactions with hsA. We observe a trend in the stability of noncovalent binding which correlates with the increasing ability of ligands **1**−**4** to promote interactions with the hydrophobic binding domains of hsA. These interactions forestall the formation of covalent interactions and influence the final concentration of hsA-coordinated Ru(III) species. The reduction potentials of **1a,b**−**4a,b** are found to be higher than NAMI-A, and noncovalent interactions do not prevent the reduction of the complexes in the presence of ascorbic acid, indicating that noncovalently protein bound Ru(II) species may be generated. By contrast, coordinated Ru(III) complexes are found to be resistant to reduction, demonstrating the potential of hsA interactions to tune the behavior of these compounds in vivo.

EXPERIMENTAL SECTION

Materials. The starting compounds $RuCl_3$ (Aldrich), pyridine (Anachemia), 4-methylpyridine (TCI America), 4-(4-nitrobenzyl)-pyridine (Alfa Aesar), diphenyl-4-pyridyl-methane (Aldrich), and DMSO (Caledon Laboratory Chemicals), as well as hsA (Aldrich), were used as purchased without further purifications. Hydrogen *trans*-bis(dimethylsulfoxide)tetrachloro-ruthenate(III), [$(DMSO)_2H$][*trans*-$Ru(DMSO\text{-}S)_2Cl_4$], and sodium *trans*-bis(dimethylsulfoxide)-tetrachloro-ruthenate(III), Na[*trans*-$Ru(DMSO\text{-}S)_2Cl_4$], were synthesized according to literature procedures.[29,30]

*PyrH[trans-$RuCl_4$(1H-Pyr)(DMSO-S)] (**1a**).* [$(DMSO)_2H$][*trans*-$Ru(DMSO\text{-}S)_2Cl_4$] (212 mg, 0.38 mmol) was dissolved in methanol (15 mL) at room temperature. Pyridine (123 μL, 1.52 mmol) was added directly to the reaction mixture. The resulting solution was stirred at room temperature for 24 h, after which a light orange-yellow precipitate was observed. The solution was filtered and washed with methanol (3 × 2 mL) and diethyl ether (3 × 2 mL). Yield: 74% $C_{12}H_{17}N_2SOCl_4Ru$ Calc. C 30.01, H 3.57, N 5.83. Found C 30.05, H 3.48, N 5.74. Melting point 179−181 °C (decomp). ^1H NMR (D_2O): δ = 8.73, 8.54, 8.00, 4.29, 2.65, −2.92, −14.51. Crystals suitable for X-ray diffraction were isolated from the reaction filtrate after cooling to −20 °C for several days.

*Na[trans-$RuCl_4$(1H-Pyr)(DMSO-S)] (**1b**).* Na[*trans*-$Ru(DMSO\text{-}S)_2Cl_4$] (105 mg, 0.25 mmol) was dissolved in acetone (8 mL) at room temperature. Pyridine (60 μL, 1 mmol) was added directly to the reaction mixture. The resulting solution was mixed for 20 min at room temperature, after which a clear orange-yellow solution was observed. The clear solution was stirred at room temperature for an additional 2.5 h, after which diethyl ether was added until precipitation was observed. The resulting red precipitate was isolated by suction filtration and washed with dichloromethane (3 × 2 mL) and diethyl

dx.doi.org/10.1021/ic202029e | *Inorg. Chem.* 2012, 51, 954−966

ether (3 × 2 mL). Yield: 77% $C_7H_{11}NSOCl_4RuNa$ Calc. C 19.87, H 2.62, N 3.31. Found C 19.82, H 2.87, N 3.37. Melting point 206−208 °C (decomp). ^{1}H NMR (D_2O): δ = 4.30, −2.89, −14.51. Crystals suitable for X-ray diffraction were isolated from the reaction filtrate.

mePyrH[trans-RuCl$_4$(1H-mePyr)(DMSO-S)] ***(2a)***. [(DMSO)$_2$H][*trans*-Ru(DMSO-S)$_2$Cl$_4$] (177 mg, 0.32 mmol) was mixed with acetone (12 mL) at room temperature. 4-Methylpyridine (123 μL, 1.26 mmol) was added directly to the reaction mixture, which immediately produced an orange precipitate. The resulting solution was stirred at room temperature for 3 h, then subsequently filtered and washed with acetone (2 × 2 mL). Yield: 86% $C_{14}H_{21}N_2SOCl_4Ru$ Calc. C 33.08, H 4.16, N 5.51. Found C 33.11, H 4.23, N 5.40. Melting point 182−184 °C (decomp). ^{1}H NMR (D_2O): δ = 8.50, 7.78, 2.57, −2.63, −3.03, −14.85. Crystals suitable for X-ray diffraction were isolated from the reaction filtrate after cooling to −20 °C for several days.

Na[trans-RuCl$_4$(1H-mePyr)(DMSO-S)] ***(2b)***. Na[*trans*-Ru(DMSO-S)$_2$Cl$_4$] (68.5 mg, 0.16 mmol) was dissolved in acetone (5 mL) at room temperature. 4-Methylpyridine (47.5 μL, 0.49 mmol) was added directly to the reaction mixture. The resulting solution was stirred at room temperature for 3 h, yielding a clear golden-yellow solution. Solvent was removed under decreased pressure to a minimal volume, then dichloromethane (10 mL) was added until precipitation was observed. The resulting mixture was filtered and washed with diethyl ether (3 × 2 mL). Yield: 81% $C_8H_{13}NSOCl_4RuNa$ Calc. C 21.98, H 3.00, N 3.20. Found C 21.67, H 3.05, N 3.33. Melting point 199−200 °C (decomp). ^{1}H NMR (D_2O): δ = −2.62, −3.01, −14.64. Crystals suitable for X-ray diffraction were isolated from the reaction filtrate after cooling to −20 °C for several days.

NbenzpyrH[trans-RuCl$_4$(1H-Nbenzpyr)(DMSO-S)] ***(3a)***. [(DMSO)$_2$H][*trans*-Ru(DMSO-S)$_2$Cl$_4$] (91 mg, 0.16 mmol) was dissolved in methanol (6 mL) at room temperature. 4(4-Nitrobenzyl)-pyridine (138 mg, 0.65 mmol) was dissolved in methanol (3 mL) and added dropwise to the reaction mixture. The resulting solution was stirred at room temperature for 3 h, after which a yellow-orange precipitate was observed. The solution was filtered and washed with methanol (2 × 2 mL). Yield: 55% $C_{26}H_{27}N_4O_5SCl_4Ru$ Calc. C 41.61, H 3.63, N 7.47. Found C 41.45, H 3.61, N 7.39. Melting point 165−167 °C (decomp). ^{1}H NMR ($CDCl_3$): δ = 8.92, 8.53, 7.85, 7.37, 5.48, 4.94, 1.55, −0.41, −1.98, −12.68. Crystals suitable for X-ray diffraction were obtained by dissolution in acetone, followed by the addition of an equal amount of dichloromethane with the resulting mixture being left at room temperature for several hours.

Na[trans-RuCl$_4$(1H-Nbenzpyr)(DMSO-S)] ***(3b)***. Na[*trans*-Ru(DMSO-S)$_2$Cl$_4$] (104 mg, 0.25 mmol) was dissolved in acetone (6 mL) at room temperature. 4(4-Nitrobenzyl)pyridine (157 mg, 0.74 mmol) was dissolved in acetone (4 mL) then added dropwise to the reaction mixture. The resulting solution was stirred at room temperature for 30 min, after which a clear golden-yellow solution was observed. Solvent was removed under decreased pressure to a minimal volume, then dichloromethane (5 mL) and diethyl ether (5 mL) were added until precipitation was observed. The solution was left standing for 10 min to complete the precipitation and was subsequently filtered and washed with diethyl ether (3 × 3 mL). Yield: 81% $C_{14}H_{16}N_2O_3SCl_4RuNa$ Calc. C 30.12, H 2.89, N 5.02. Found C 30.07 H 2.80, N 4.98. Melting point 156−158 °C (decomp). ^{1}H NMR (D_2O): δ = 6.75, 4.85, −0.30, −3.05, −14.63. Crystals suitable for X-ray diffraction were isolated from product dissolved in ethyl acetate at elevated temperatures followed by gradual cooling to room temperature.

dibenzPyrH[trans-RuCl$_4$(1H-dibenzPyr)(DMSO-S)] ***(4a)***. [(DMSO)$_2$H][*trans*-Ru(DMSO-S)$_2$Cl$_4$] (204 mg, 0.37 mmol) was dissolved in methanol (10 mL) at room temperature. Diphenyl-4-pyridyl-methane (537 mg, 2.19 mmol) was dissolved in methanol (10 mL) then added dropwise to the reaction mixture. The resulting clear orange solution was stirred at room temperature for 30 min, affording a clear golden-yellow solution. Solvent was removed under reduced pressure until a yellow precipitate was observed. The solution was subsequently filtered and washed with methanol (3 × 2 mL). Yield: 40% $C_{36}H_{37}N_2OSCl_4Ru$ Calc. C 54.83, H 4.73, N 3.55. Found C 54.92, H 4.79, N 3.59. Melting point 143−145 °C (decomp). ^{1}H NMR ($CDCl_3$): δ = 8.84, 7.64, 7.52, 6.64, 6.46, 6.24, 5.09, 1.52, 1.01, −2.40, −13.37.

Na[trans-RuCl$_4$(1H-dibenzPyr)(DMSO-S)] ***(4b)***. Na[*trans*-Ru(DMSO-S)$_2$Cl$_4$] (63.8 mg, 0.15 mmol) was dissolved in acetone (5 mL) at room temperature. Diphenyl-4-pyridyl-methane (111 mg, 0.45 mmol) was dissolved in acetone (2 mL) then added dropwise to the reaction mixture. The solution was stirred at room temperature for 3 h, resulting in a clear golden-yellow solution. Solvent was removed under decreased pressure to a minimal volume, then dichloromethane (10 mL) was added until precipitation was observed. The resulting mixture was filtered, yielding an orange powder which was dried at 75 °C for 3 h. Yield: 58% $C_{20}H_{21}NOSCl_4RuNa$ Calc. C 40.76, H 3.59, N 2.38. Found C 40.40, H 3.41, N 2.07. Melting point 225−227 °C (decomp). ^{1}H NMR (D_2O): δ = 6.59, 6.36, 5.38, 4.87, 0.98, −3.13, −14.81. Crystals suitable for X-ray diffraction were isolated from an ethyl acetate solution upon cooling to −20 °C for several days.

Crystallographic Structure Determination. Single crystal X-ray diffraction analysis was performed on a Bruker SMART diffractometer equipped with an APEX II CCD area detector fixed at a distance of 6.0 cm from the crystal and a Mo Kα fine focus sealed tube (λ = 0.71073 nm) operating at 1.5 kW (50 kV, 30 mA) and filtered with a graphite monochromator. The temperature was regulated using an Oxford Cryosystems Cryostream. Structures were solved using direct methods (SIR92) and refined by least-squares procedures in CRYSTALS.[31] Diagrams of **1a**,**b**, **2a**,**b**, **3a**,**b** and **4b** were generated by ORTEP-3 for Windows (v. 2.00[32] and rendered using POV-Ray (v. 3.6.1).[33] Crystal data, data collection parameters, and details of structure refinement for compounds **1a**,**b**, **2a**,**b**, **3a**,**b** and **4b** are listed in Table 1.

Electrochemical Measurements. Cyclic voltammograms were recorded on a Princeton Applied Research potentiostat/galvanostat Model 263A, equipped with a Ag/AgCl (3 M KCl) reference electrode, a platinum disk working electrode and a platinum disk counter electrode. All spectra were collected in an aqueous buffer consisting of 50 mM NaH_2PO_4, 150 mM NaCl, and 20 mM $NaHCO_3$, henceforth "physiological buffer". $K_4[Fe(CN)_6]$ was used as a calibration. Measurements were performed using 5 mM concentrations of each complex in 5 mL of solvent using a 100 mV/s scan rate. All scans were conducted under these conditions unless otherwise noted.

Preparation of EPR Samples. *Complexes in Buffer.* Compounds were dissolved in physiological buffer to give a concentration of 3 mM, and incubated at 37 °C. Aliquots of 210 μL were withdrawn at the following time points: 0, 10, 20, 30, 60, and 120 min. Each sample was promptly mixed with 30% by volume of glycerol, which acted as a glassing agent, and frozen in liquid nitrogen.

Complexes with hsA. To 600 μL of a 0.75 mM solution of hsA in physiological buffer was added 600 μL of a 1.5 mM solution of each complex also in physiological buffer. The combined solution was then diluted to 4 mL with physiological buffer and incubated at 37 °C for one of the following time periods: 0, 10, 20, 30, 60, and 120 min. Each 4 mL solution was concentrated down to a volume of less than 200 μL using an Amicon centrifugal filter unit (molecular-weight cutoff 30 kDa) by centrifuging at 8 °C and 4500 rpm for 30 min, or until a volume of less than 200 μL was attained. The resulting filtered product was then mixed with 90 μL of glycerol and diluted to a final volume of 300 μL with physiological buffer, and finally transferred to an EPR tube and immediately frozen in liquid nitrogen.

Complexes with Ascorbic Acid in Buffer. A 1 mM solution of each complex was prepared in physiological buffer at 25 °C . Ascorbic acid was subsequently added to give a concentration of 1 mM. The resulting solutions were then incubated at 37 °C for either 0 or 120 min. Aliquots of 210 μL were mixed with 30% glycerol by volume, and transferred to an EPR tube and immediately frozen in liquid nitrogen.

Complexes with hsA and Ascorbic Acid. A 1 mM solution of each complex was mixed with a 0.5 mM solution of hsA and incubated at 37 °C for either 0 or 120 min. After incubation and isolation of the protein bound fractions, ascorbic acid (15 mM) was added to the mixture, giving an acid concentration of 1 mM. Protein-bound

Table 1. Crystal Data and Details of Data Collection and Refinement for Compounds 1a,b, 2a,b, 3a,b, and 4b

	1a	1b	2a	2b	3a	3b	4b
empirical formula	$C_{13.5}H_{20}N_2SO1.5Cl_4Ru$	$C_{5.25}H_9NS_{0.75}O_{1.12}Cl_3Ru_{0.75}Na_{0.75}$	$C_{14}H_{21}N_2SOCl_4Ru$	$C_8H_{17}NS\ O_{2.5}Cl_4RuNa$	$C_{28}H_{27}N_4SO_3SCl_4Ru$	$C_{18}H_{24}N_2SO_3Cl_4RuNa$	$C_{28}H_{37}NSO_3Cl_4RuNa$
M (g mol^{-1})	509.27	324.09	508.28	465.16	750.47	646.34	765.54
space group	triclinic $P\bar{1}$	trigonal $P3121$	triclinic $P\bar{1}$	orthorhombic $Fdd2$	ortho-rhombic $Pca21$	triclinic $P\bar{1}$	triclinic $P\bar{1}$
a (Å)	7.351	13.143	9.273	23.882	27.495	8.922	11.468
b (Å)	8.532	13.143	15.340	26.026	7.945	9.724	12.632
c (Å)	15.098	19.609	15.871	11.443	14.515	14.839	14.731
α (deg)	88.243	90	99.532	90	90	99.805	93.075
β (deg)	79.191	90	105.574	90	90	90.656	109.88
γ (deg)	88.959	120	107.318	90	90	96.222	116.24
V (Å^3)	978.22	2933.6	2000.8	7112.9	3171.0	1260.5	1746.81
Z	2	8	4	16	4	2	2
ρ_{calc} (g cm^{-3})	1.729	1.467	1.687	1.737	1.572	1.703	1.455
μ (g mm^{-1})	1.460	1.464	1.425	1.620	0.939	1.178	0.862
λ (Å)	0.71073	0.71073	0.71073	0.71073	0.71073	0.71073	0.71073
T (K)	298	150	298	150	298	150	298
goodness of fit	1.4583	1.0358	1.4190	1.8772	1.313	1.050	1.0196
R_1	0.0319	0.0637	0.0292	0.0395	0.0532	0.0348	0.0497
wR_2	0.0376	0.0663	0.0311	0.0559	0.0442	0.0284	0.0637

fractions were separated by ultrafiltration as described above for the complexes incubated with hsA in buffer.

EPR Measurements and Simulations. EPR spectra were collected at X-band (9.3−9.4 GHz) using a Bruker EMXplus spectrometer with a PremiumX microwave bridge and HS resonator. Low temperature (20 K) measurements were performed using a Bruker ER 4112HV helium temperature-control system and continuous-flow cryostat. So that the intensities of EPR signals from Ru(III) species in each solution after different incubation times could be compared, sample preparation and spectroscopic parameters were unchanged for each experiment. EPR samples (300 μL) for each series of incubation times were drawn from a common stock solution. The design of the Bruker cryostat system, which contains a quartz-insert tube holder, ensures reproducible sample placement within the EPR resonator. Consequently, variation in instrument sensitivity between measurements was minimal, and automatic tuning of the spectrometer gave a Q-factor of 6500 ± 10%. To monitor the accuracy of this approach, a reference compound 5,10,15,20-tetrakis(4-sulfonatophenyl) porphyrinato iron(III) chloride (FeTPPS) was added to several samples. In each case, the original samples were briefly thawed and 20 μL of a 3 mM solution of FeTPPS in buffer was added. The samples were then refrozen in liquid nitrogen and their EPR spectra remeasured. FeTPPS gives an axial EPR spectrum with a characteristic signal at $g_{\perp}$ = 5.8, and this feature was used as a reference to compare the overall intensity of Ru(III) signals at different time points. In experiments with hsA, the distinctive EPR signal from a minor Fe(III) human serum transferrin impurity at g = 4.3 also provided a reference for normalizing the Ru(III) EPR signal sensitivity.

All spectra were simulated using the program Bruker WinEPR Simfonia which efficiently produces accurate results for most S = 1/2 systems. A manual, iterative fitting procedure was employed to analyze overlapping spectra observed when multiple Ru(III) species were present in a particular sample. The Matlab-based simulation package EasySpin[34] was also used to reproduce the simulations of some spectra and the results were identical to those using WinEPR Simfonia.

RESULTS AND DISCUSSION

Synthesis. Compounds **1a**−**4a** and **1b**−**4b** were synthesized using procedures based on those reported for NAMI-A and NAMI, respectively.[30,35] Initial synthesis of the bis-DMSO complexes, $[(DMSO)_2H][trans\text{-}Ru(DMSO\text{-}S)_2Cl_4]$, and Na-$[trans\text{-}Ru(DMSO\text{-}S)_2Cl_4]$ was followed by addition of the ligands **1**−**4** to give **1a**−**4a**, and **1b**−**4b** respectively in good yield. The identity and purity of these compounds was confirmed by elemental analysis, NMR, EPR, and X-ray crystallography.

Although the original patents describing NAMI-A and related complexes encompass compounds with a variety of heterocyclic nitrogen ligands,[36] synthesis and, particularly, characterization of these species has been somewhat limited. In the case of NAMI-A analogues with different heterocyclic nitrogen donor ligands, a number of imidazole-based derivatives have been reported,[37,38] along with a modest number of compounds with other types of nitrogen heterocycles, including thiazoles,[39,40] triazoles,[41−43] pyridines,[7,44−50] and various other azole ligands.[41,44,51] Of the compounds described here, synthesis of **1a**,**b** and **2a**,**b** have been previously reported.[7,46,48,50] However, aside from NMR and UV−vis studies of **2a**,[50] only **1a** has been fully structurally characterized.[46] No NAMI-A derivatives similar to **3a**,**b** and **4a**,**b** have been reported to date. As described here, we have characterized all eight compounds **1a**,**b**−**4a**,**b** prior to studying their aqueous solution behavior, protein interactions, and electrochemistry.

Crystal Structures. The structures of compounds **1a**,**b**, **2a**,**b**, **3a**,**b**, and **4b** determined by X-ray crystallography are shown in Figure 3. The significant differences in the solvent

dx.doi.org/10.1021/ic202029e | Inorg. Chem. 2012, 51, 954−966

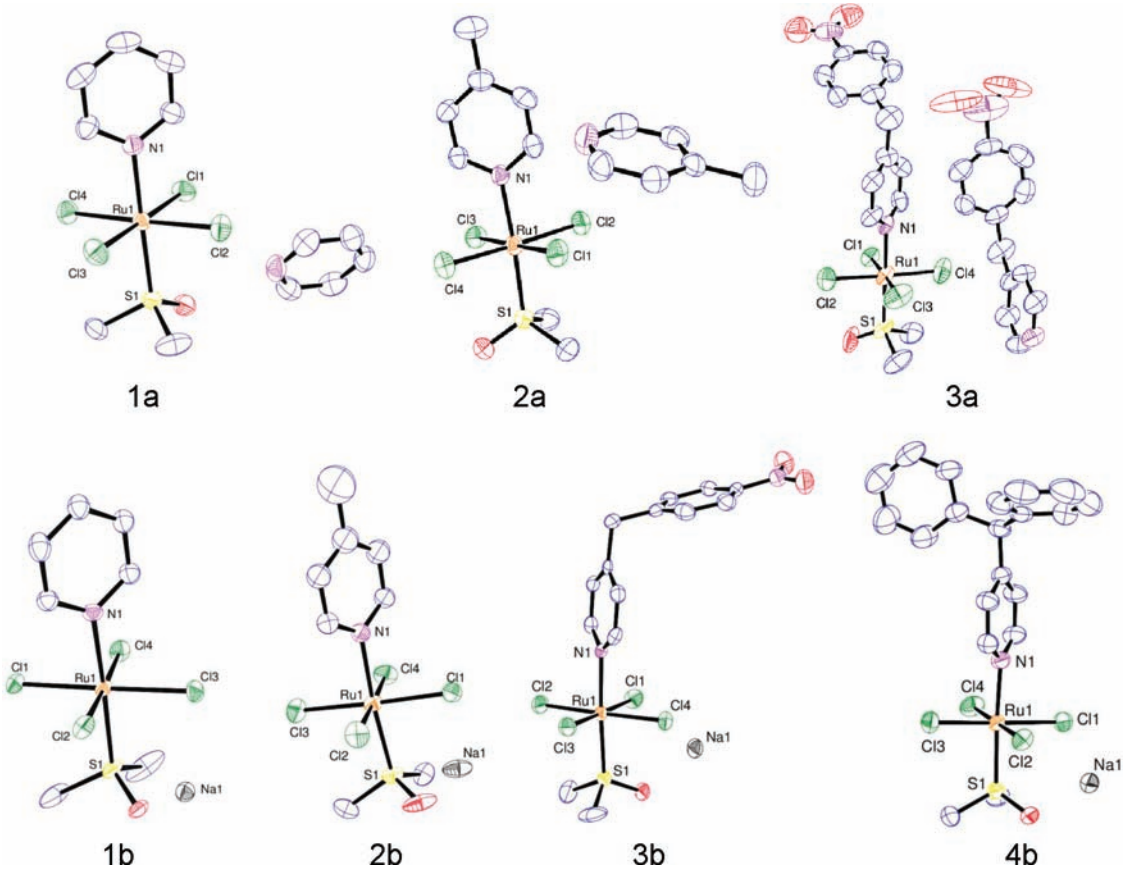

Figure 3. Crystal structures of compounds **1a,b**, **2a,b**, **3a,b**, and **4b**.

preferences of the azole ligands and counterions required different approaches to obtain crystals suitable for X-ray diffraction studies. Crystals of complexes **1a**, **1b**, **2a**, and **2b** were all isolated directly from the reaction filtrate after standing for several days at low temperature. For **3a**, dissolution in acetone followed by the addition of dichloromethane (1:1) resulted in X-ray quality crystals within minutes. Single crystals of **3b** were obtained by dissolution in ethyl acetate at elevated temperatures followed by a very gradual cooling period. Despite numerous attempts using a wide array of conditions and solvent systems, no crystals suitable for X-ray diffraction studies of compound **4a** were attained. However, crystals of **4b** were obtained from a solution of ethyl acetate after several days at low temperature. The crystal structure of **1a** has been reported previously,[45] and we find metrical parameters that agree with this earlier study within experimental error. To our knowledge, none of the other compounds have been characterized crystallographically.

For all of the structures solved, similar distorted octahedral geometry around the ruthenium(III) metal center is observed. In all cases the DMSO ligand is coordinated via the sulfur atom while the pyridine ligand is coordinated through the heterocyclic nitrogen. An equatorial plane of four chlorides completes the coordination sphere. This type of coordination environment around the ruthenium metal center has been well documented, and is typical of analogous complexes.[7,13,30,37,40,41,47,52]

The bond lengths for all of the complexes are listed in Supporting Information, Table S3. The metal−ligand bond lengths of all the synthesized complexes are similar to NAMI-A[40] and its sodium-compensated analogue NAMI.[30] For the crystallographically characterized complexes (**1a,b**, **2a,b**, **3a,b**, **4b**), the average Ru−N bond distance (2.11 Å) is similar to the reported value for NAMI (2.081 Å) and NAMI-A (2.099 Å). The corresponding average Ru−S bond distances (2.30 Å) are also very similar to the values for NAMI (2.296 Å) and NAMI-A (2.293 Å). Ru−Cl bond distances were evaluated individually across all the complexes, with the resulting average Ru−Cl bond distance of 2.355 Å close to those of NAMI-A (2.353 Å) and NAMI (2.342 Å).

In the case of the sodium salts, all of the structures (**1b**−**4b**) were solved as dimers, since the sodium cations exhibit a distorted octahedral geometry between chloride ligands on neighboring ruthenium centers and cocrystallize with solvent molecules. Low temperature collection of diffraction data was required to prevent desolvation of crystals of **1b**, **2b**, and **3b**, which otherwise reduced the crystals to powder. Similar behavior has been reported for crystals of NAMI.[30] The bridging oxygen atoms in **1b** and **2b** and the free oxygen atom in **2b** were modeled as water molecules. Determination of the identity of these water molecules was complicated by the vibrational motion present in both **1b** and **2b**, which is evident in the pyridine rings and the anisotropic temperature factors of the equatorial chlorides. Lastly, for **3b** and **4b**, cocrystallizing ethyl acetate molecules were modeled; with relative ease in the case of **3b** and with significant disorder for **4b**, which required two solvent molecules being modeled with partial occupancy.

EPR of Aqueous Solution Behavior. Before studying the protein interactions of compounds **1a,b**−**4a,b**, it was first necessary to characterize their ligand-exchange processes in physiological buffer. Principally, we wanted to determine whether their fundamental solution behavior was similar, and

dx.doi.org/10.1021/ic202029e | *Inorg. Chem.* 2012, 51, 954−966

whether it would play a significant role in the rate of formation of interactions with hsA.

The paramagnetic Ru(III) (low-spin d^5, $S = 1/2$) centers of these compounds facilitate EPR studies to determine the symmetry and ligand fields of the complexes as they undergo ligand-exchange processes. Analysis of g values and signal intensities from frozen solutions of the compounds enables identification of species produced by ligand exchange and determination of the rates of these processes. Furthermore, processes that produce diamagnetic species, such as reduction to give Ru(II) (low-spin d^6, $S = 0$) or dimerization to give antiferromagnetically coupled bimetallic species, can be monitored via loss of overall signal intensity because of the production of "EPR silent" species.

Under the physiologically relevant experimental conditions used in these studies (pH 7.4, 37 °C), Ru(III) complexes generally exhibit relatively slow ligand exchange.[53] Thus, we tracked the concentration changes of various Ru(III) complexes after incubation times up to 2 h, by freezing the solutions in liquid nitrogen at selected time points. EPR measurements of these frozen solutions then provide a "snap shot" of the species present and their relative concentrations. Frequently, ligand exchange processes gave complex mixtures of Ru(III) species, which exhibited overlapped EPR spectra, requiring deconvolution for analysis. This was achieved by simulating the spectra of each individual species to determine a set of g values and line widths. Each spectrum was then multiplied by a weighting factor, correlating with the concentration of the Ru(III) species in the solution, before adding together the components from all of the identified species to reproduce the experimental spectrum. To ensure a unique solution was determined for the spectral parameters of each overlapped species, simulations were performed for all of the incubation time points simultaneously, with only the weighting factor for each spectral component varied.

To compare the solution behavior of **1a**,**b**−**4a**,**b**, the compounds were incubated in physiological buffer (pH 7.4) at 37 °C for time periods of 0, 10, 20, 30, 60, and 120 min before freezing in liquid nitrogen and measurement by EPR. The resulting EPR spectra are shown in Figure 4 for **1a** and **4b**, and in the Supporting Information, Figures S1 and S2 for the remaining complexes. For each complex a well-resolved uniaxial spectrum was observed prior to incubation at 37 °C, as expected for mononuclear low-spin Ru(III) complexes with tetragonal symmetry, indicating detection of the parent compound in each case. The g values of the parent compounds, determined by simulation (Figure 4, right-hand panels and Supporting Information, Figures S5−S12), are similar with $g_\perp$ = 2.43−2.44 and $g_\parallel$ = 1.75−1.80, as expected since the substituents on the pyridine ligands do not affect the ligand field of the Ru(III) ion significantly. In the case of compounds **3a** and **4a**, the spectra attained before incubation in buffer at 37 °C are not strictly uniaxial. Relatively poor water solubility results in some aggregated complexes in solution. This produces a weak, broad EPR signal which distorts the axial peak from the dissolved complexes. By contrast, their sodium analogues, **3b** and **4b**, are readily soluble in aqueous media and thus do not display this signal.

With incubation at 37 °C, a new uniaxial EPR signal was observed in measurements of each complex with $g_\perp$ = 2.30−2.31 and $g_\parallel$ = 1.87−1.88 (EPR spectra labeled as **1a**-C3 and **4b**-C3 in Figure 4, and correspondingly for other complexes in Supporting Information, Figures S5−S12), which steadily

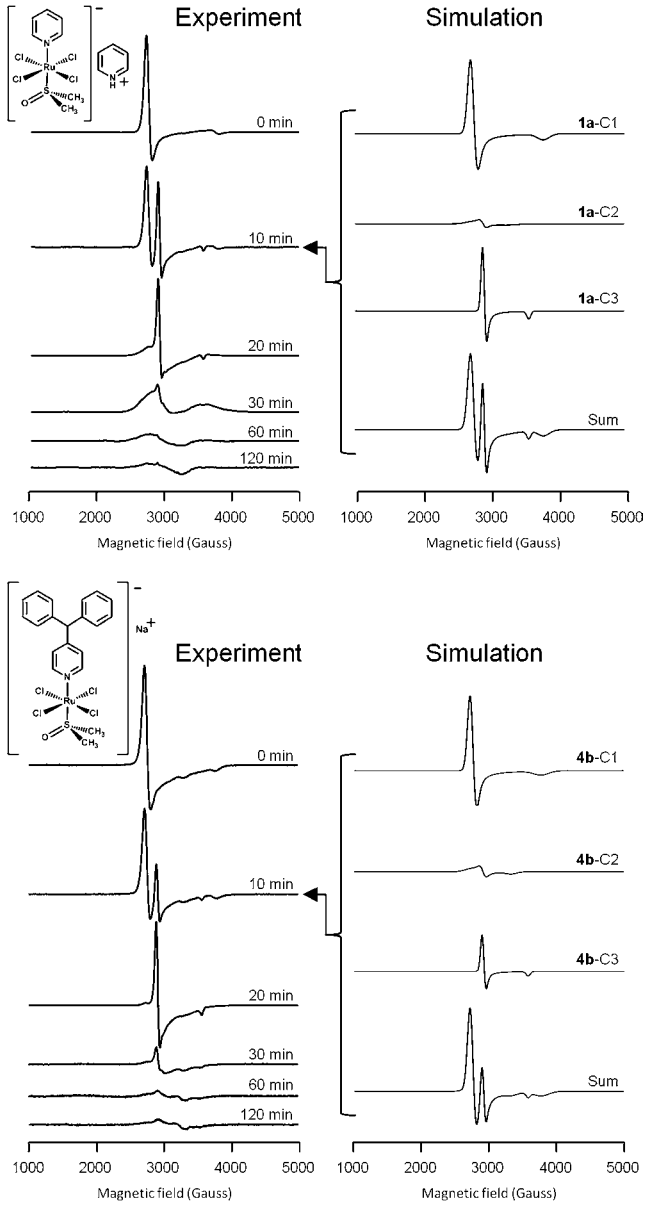

Figure 4. EPR measurements of **1a** and **4b** incubated in physiological buffer at 37 °C, and spectral deconvolution of spectra collected after 10 min of incubation. As shown by the spectral simulations, two aquated species are generated, with the axially symmetric species **1a**-C3 and **4b**-C3, generated by loss of DMSO, dominating in both cases. Smaller contributions from the lower symmetry species, **1a**-C2 and **4b**-C2 are generated by loss of Cl^-. **Experimental parameters:** frequency = 9.38 GHz, microwave power = 2.0 mW, time constant = 40.96 ms, modulation amplitude = 6 G, average of five 2-min scans. For EPR measurements of the solution behavior of other complexes, see Supporting Information, Figures S1 and S2. For spectral deconvolution of spectra collected at each incubation time point for each complex, see Supporting Information, Figures S5−12. For spectral parameters used in each simulation see Supporting Information, Table S1.

replaced the signals from the parent compounds, indicating the loss of one of the axial ligands. Nitrogen donor ligands are generally considered to be kinetically inert under physiological conditions (pH 7.4),[15] implying that the axial DMSO ligand of the complexes exchanges with water in each case. However, to confirm this, we performed NMR measurements of the sodium-compensated complexes **1b**−**4b**, following incubation in buffer

dx.doi.org/10.1021/ic202029e | Inorg. Chem. 2012, 51, 954−966

for 0, 2, and 24 h (Supporting Information, Figures S30−S33). Only trace amounts of free pyridine ligands were detected even after 24 h, confirming [*trans*-$RuCl_4$(1*H*-L)(H_2O)]$^-$ as the dominant product in solution after 10 min of incubation.

Simulations of the spectra obtained after 10 and 20 min of incubation for each complex at 37 °C reveal a smaller contribution from a third species, which exhibits a rhombic EPR spectrum, g = [2.41−2.46, 2.25−2.31, 2.01−2.07] (Figure 4, right-hand panels, Supporting Information, Figures S5−S12). The lower symmetry species observed are consistent with aqueous exchange of an equatorial chloride ligand, which produces a second monoaqua species $RuCl_3H_2O$(1*H*-L)-(DMSO-*S*) (**1a**-C2 and **4b**-C2 in Figure 4). The lower signal intensity from this species in each case indicates that Cl^- exchange occurs concurrently with loss of DMSO, but at a significantly slower rate. The g values for each compound (**1a,b**−**4a,b**), and their monoaqua derivatives ([**1a,b**−**4a,b**]-C2 and [**1a,b**−**4a,b**]-C3) are listed in the Supporting Information, Table S1.

Further incubation of the compounds in solution leads to a considerable decrease in the overall EPR signal intensity. Since these buffer solutions do not contain significant reducing agents, redox processes leading to EPR silent Ru(II) (d^6, S = 0) complexes are not responsible for this effect. Instead, oligomerization of the aquation products to give oxo- or hydroxo-bridged species likely explains the loss of paramagnetic species, since antiferromagnetic coupling between adjacent Ru(III) centers can produce species with a net spin of S = 0. This behavior has been previously reported for NAMI-A, and is accompanied by a distinct change in the color of the solution from yellow to dark brown.[15,17] A similar phenomenon was also observed for each of the pyridine complexes described in this work. Although the EPR signals are significantly attenuated after longer incubation periods, it is still possible to observe ongoing changes in the spectra. This indicates a small proportion of the complexes remain as mononuclear Ru(III) species and continue exchanging Cl^- ligands to give polyaqua species. However, the very low concentration of these species indicates that they are unlikely to play a significant role in the activity of the compounds.

Overall, the rates of ligand exchange processes do not vary dramatically depending either on the axial ligands or the counterions. In every case the axial monoaqua complex dominates after 10 min of incubation at 37 °C, and the overall signal intensity is significantly reduced after 30 min. The spectroscopic parameters of each complex are also relatively similar, as expected given the similar ligand-fields provided by the axial ligands in each case. Furthermore, changing the counterions did not affect the EPR spectra noticeably. Thus, the spectra shown for **1a** and **4a** in Figure 4 are similar to those observed for the other compounds (Supporting Information, Figures S1−S2). The only exception was **4a**, which was relatively insoluble in aqueous media because of its hydrophobic dibenzPyr axial ligand and dibenzPyrH counterion, requiring 20% DMSO for sufficient dissolution. The resulting EPR spectra, although showing contributions from the parent compound and monoaqua complexes in solution, are dominated by a broad signal, which is relatively unchanged even following longer incubation periods, and likely arises from aggregated complexes. This was confirmed by measurement of a powder sample of **4a**, which gave a broad signal matching that seen in the frozen solution experiment (data not shown). By contrast, the sodium analogue, **4b**, dissolves readily in buffer and shows the typical speciation behavior.

The aqueous solution behavior of NAMI-A has been studied extensively by a variety of techniques, demonstrating that aquation products and oligomers predominate after incubation of the complex in aqueous buffer solutions at pH 7.4.[15−17,19−21,41,54] We have previously reported EPR characterization of NAMI-A in physiological buffer, and find speciation and ligand-exchange rates that are very similar to those of the pyridine complexes described in this work.[17] This further demonstrates that although the axial azole ligands influence the electrochemistry and biomolecule interactions of this family of compounds, they do not impact significantly on their fundamental aqueous solution behavior. This is an important observation since solutions of these types of compounds are frequently prepared in physiological saline, prior to intravenous administration. Thus, the time taken between the preparation of these solutions and infusion determines the actual compounds delivered to patients, significantly affecting in vivo behavior and activity.

EPR of Interactions of Complexes with hsA. As the dominant protein in the circulatory system, hsA has been identified as the agent responsible for the binding of many drugs and their delivery to sites of disease.[55,56] A number of studies have characterized covalent interactions of NAMI-A and Keppler-type complexes with hsA, because of ligand exchange with amino acid side chains, particularly histidine imidazoles.[22,25,26,57] There is some debate regarding the effects of these interactions on the bioavailability and antiproliferative activity of NAMI-A and other Ru(III) anticancer compounds.[24,26] However, recent studies of NAMI-A bound to bovine serum albumin demonstrate that the protein-bound complex exhibits high antimetastatic activity.[24]

The hydrophobic regions in subdomains IIA and IIIA of hsA are prominent molecular binding sites and are the most probable locations of noncovalently bound ruthenium species.[56,58] We have previously used EPR methods to show that NAMI-A, and the monoaqua complex formed by DMSO exchange, both rapidly form noncovalent interactions with hsA.[17] Although these species are predominant shortly after dissolution in the presence of hsA, or in whole human serum, they are steadily converted to covalently bound species with further incubation via ligand exchange with amino acid side chains.[17]

The complexes **1a,b**−**4a,b** were incubated for 0, 10, 20, 30, 60, and 120 min at 37 °C in buffer solutions of hsA. Protein-bound fractions were then isolated by ultrafiltration, with a molecular-weight cutoff of 30 kDa, frozen in liquid nitrogen, and studied by EPR. The resulting spectra for each incubation time are shown in Figure 5 for **1a** and **4a**, and in Supporting Information, Figures S13−S20 for the other complexes. This approach allows us to observe exclusively hsA-bound Ru(III) species while excluding contributions from free complexes in solution, and has been used in earlier studies to identify both covalent and noncovalent binding interactions of NAMI-A and the Keppler-type complexes KP1019 and KP418 with hsA.[17,21]

For each of the pyridine complexes **1a,b**−**4a,b** incubated with hsA, EPR measurements after short incubation periods reveal signals that correspond to the parent compounds and the monoaqua complexes ([**1a,b**−**4a,b**]-C2 and [**1a,b**−**4a,b**]-C3) that were observed in the buffer solution experiment described previously. However, since only protein bound fractions are present, these signals are due to complexes bound to hsA

dx.doi.org/10.1021/ic202029e | *Inorg. Chem.* 2012, 51, 954−966

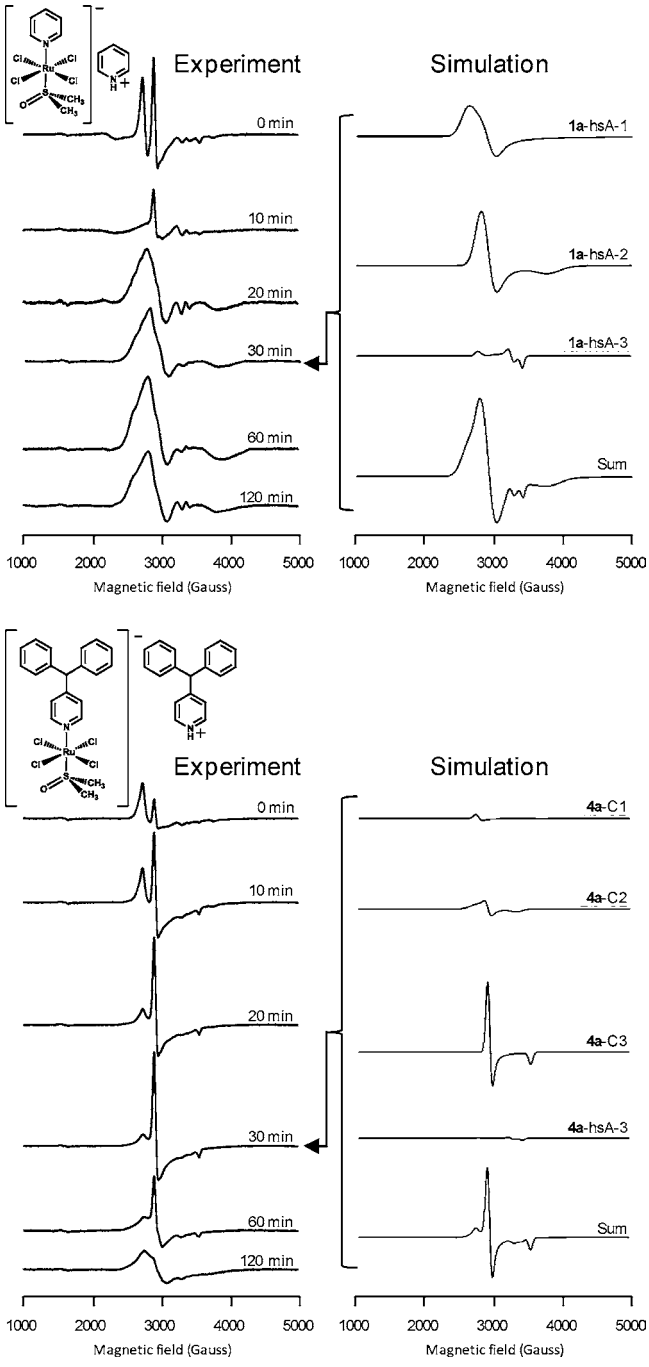

Figure 5. EPR spectra of **1a** and **4a** incubated with hsA in physiological buffer at 37 °C, and spectral deconvolution of spectra collected after 30 min of incubation. **Experimental parameters:** frequency = 9.38 GHz, microwave power = 2.0 mW, time constant = 40.96 ms, modulation amplitude = 6 G, average of five 2-min scans. For EPR measurements of hsA binding behavior of other complexes, see Supporting Information, Figures S3–S4. For spectral deconvolution of spectra collected at each incubation time point for each Ru(III) species, see Supporting Information, Figures S13–S20. For spectral parameters used in each simulation see Supporting Information, Table S2.

without ligand exchange with the protein, that is, noncovalently bound species. The strong signals observed in each case, even prior to incubation at 37 °C, demonstrate that these interactions form readily with hsA and initially predominate in solution.

After longer incubation periods the EPR spectra from all of the pyridine complexes are increasingly dominated by two overlapping broader signals, which are not observed in the buffer solution experiments, with g values of $g_{\perp}$ = 2.33–2.40 and $g_{\parallel}$ = 1.76, and g = [2.56–2.59, 2.24–2.30, 1.76–1.78]. The distinct g values of these species indicate new Ru(III) ligand environments due to protein interactions. This reflects coordination to amino acid side chains, most probably histidine imidazoles, as suggested in previous studies.[17,21,25,57,59,60] The hsA protein has upward of 5 surface histidine residues that are capable of coordinating to exogenous species,[61] and previous studies have demonstrated that up to 5 equivalents of NAMI-A can bind to the protein.[59,60] In our experiments the ratio of complex to hsA molecules was 2:1. This increases the possibility of different coordination modes, as compared to a 1:1 ratio, but was not an excessive concentration for noncovalent interactions. The strong EPR signals observed from these species indicate protein coordination is highly favored, likely giving more than one Ru(III) complex coordinated per protein molecule. Furthermore, EPR measurements of the filtrate after separation of protein bound fractions did not show detectable concentrations of Ru(III).

As shown by the spectral deconvolution of the EPR spectrum of **1a** after 30 min of incubation with hsA, (Figure 5, right-hand panel, and for the other pyridine complexes in Supporting Information, Figures S13–S20), one of these species has a uniaxial EPR spectrum (**1a**-hsA-2), indicating coordination at the labile axial site, while the other has rhombic symmetry (**1a**-hsA-1) demonstrating coordination to an equatorial position previously occupied by chloride in the parent complex. These observations are similar to those reported for NAMI-A, indicating that the pyridine complexes have the same types of covalent interactions with hsA.[17] However, as shown by the corresponding spectra for **4a** (Figure 5), the chemical structure of the pyridine ligands strongly affects the rates that the various protein-bound species form, and their relative concentrations.

A third protein-coordinated species is also evident for each complex (**1a**-hsA-3 and **4a**-hsA-3 in Figure 5, and corresponding species in Supporting Information, Figures S13–S20) which is characterized by a sharp, rhombic EPR spectrum with g = [2.42, 2.06, 1.96]. Although the EPR signal intensity of this species is much lower than the main protein-bound species described above, it forms more rapidly, essentially reaching its maximum concentration before incubation at 37 °C. The smaller g-value dispersion and narrow line widths of this species demonstrate a different ligand environment from the other protein-coordinated species. Human serum albumin has one free cysteine (Cys-34) which has a reactive thiol available for coordination under physiological conditions,[62,63] and we suggest that coordination of the pyridine complexes described here to this residue is a possible source of this signal. This species has also been observed for NAMI-A incubated with hsA, exhibiting a very similar EPR signal.[17] Furthermore, interactions of platinum-based drugs with Cys-34 of hsA have been reported,[62] indicating that this could be a favorable mode of coordination for ruthenium complexes.

The incubation time-dependence of the EPR signals from **1a** with hsA closely resembles that of NAMI-A,[17] as might be expected given the similar propensity of the imidazole and pyridine ligands to form hydrophobic interactions with hsA. In both cases, EPR measurements reveal the formation of noncovalently bound species prior to incubation. After 10 min of incubation at 37 °C, these species have mostly

dx.doi.org/10.1021/ic202029e | Inorg. Chem. 2012, 51, 954–966

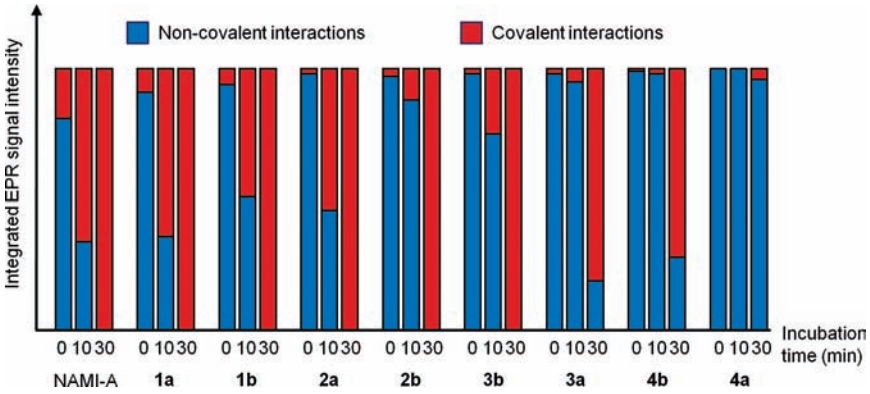

Figure 6. Relative fractions of covalently and noncovalently hsA bound Ru(III) complexes following 0, 10, and 30 min of incubation at 37 °C, as determined from integrated EPR signal intensity.

disappeared, and by 20 min they are completely replaced by covalently bound complexes whose concentration continues to increase, reaching a maximum after about 1 h (Figure 5). Almost identical behavior is observed for the sodium compensated complex, **1b** (Supporting Information, Figure S4b), demonstrating that the counterions do not significantly influence the protein interactions in this case. These results indicate that by using fresh solutions of each complex for intravenous treatment, covalently bound species will rapidly predominate in vivo. By contrast, the mePyr analogues **2a** and **2b**, show significant concentrations of the monoaqua complex, *trans*-$RuCl_4$(1*H*-mePyr)(H_2O), noncovalently bound to the protein after 10 min of incubation (Supporting Information, Figures S15b and S16b), demonstrating that these species are significantly stabilized toward noncovalent interactions with hsA by the presence of the methyl group at the 4 position as compared to **1a** and **1b**. This effect is even more pronounced in the other pyridine derivatives, with the NbenzPyr complexes **3a** and **3b** showing dominant noncovalent interactions after 20 min of incubation (Supporting Information, Figures S17c–S18c), and the diphenPyr complexes **4a** and **4b** found primarily in noncovalent interactions after at least 60 and 30 min of incubation with hsA at 37 °C respectively (Figure 5, right-hand panel, and Supporting Information, Figures S19e–S20d).

The relative concentrations of covalently and noncovalently hsA-bound Ru(III) complexes was determined for **1a**,**b**–**4a**,**b** over the first 30 min of incubation by first simulating the overlapping spectral signals using weighting factors, as described in the previous section (Figure 5 and Supporting Information, Figures S13–S21). Using the double integration values of these simulated spectra gave the relative concentrations of each of the species present following incubation of **1a**,**b**–**4a**,**b** for 0, 10, and 30 min at 37 °C. As summarized in Figure 6, these calculations reveal a trend in the stability of the noncovalent interactions of **1a**,**b**–**4a**,**b** with hsA that correlates with the ability of their axial ligands to facilitate interactions with the hydrophobic binding domains of hsA. As shown by the relative proportions of covalently and noncovalently bound Ru(III) species, the axial ligands increase the persistence of noncovalently bound species according to diphenPyr > NbenzPyr > mePyr > Pyr. Figure 5 highlights the dramatic difference between the protein interactions of **1a** and **4a**. The Pyr complex (**1a**) is observed solely as covalently bound species after 30 min of incubation with hsA, whereas the diphenPyr complex (**4a**) still shows a contribution from noncovalently bound species after 120 min. Spectral deconvolutions for all protein-bound species at all incubation time points, in addition to those in Figure 5, are shown in the Supporting Information, Figures S13–S20.

The sodium compensated analogues of the complexes described here are desirable in consideration of their pharmaceutical potential because of the potential toxicity of the pyridine counterions in **1a**–**4a**. Furthermore, as described above, the sodium salts also have significantly improved solubility in aqueous solution, which is particularly important when highly hydrophobic ligands such as diphenPyr are used. However, the counterion choice does not seem to significantly impact the interactions with hsA. The notable exception to this is in the behavior of the diphenPyr compounds, where the sodium compensated complex (**4b**) very rapidly forms noncovalent interactions with the protein, while the diphenpyrH salt (**4a**) initially exhibits relatively low levels of hsA-bound species. This is consistent with the relative insolubility of **4a** in aqueous solution, which leads to the formation of aggregated species, as described above. With further incubation, the signals from noncovalently bound **4a** increase significantly, demonstrating that the protein interactions effectively solubilize the complex.

While it is clear that increased derivatization of the pyridine ligands forestalls the formation of covalent interactions with hsA, by stabilizing noncovalent binding, it also influences the final concentrations of coordinated Ru(III) species (Figures 5 and 6, Supporting Information, Figures S13–S20). The Pyr compounds **1a** and **1b** show strong, and similar intensity, EPR signals from hsA-coordinated complexes after 2 h of incubation at 37 °C. Comparison with the mePyr complexes **2a** and **2b** shows signal intensities which are 40 and 60% lower, respectively, after the same incubation time. This effect is even more pronounced for the NbenzPyr and diphenPyr analogues with the concentrations of the analogous species reduced by 70–80%. Formation of covalent interactions is slow, as expected for ligand exchange reactions under these conditions,[53] but is thermodynamically favored and thus dominates at longer time periods. However, these data indicate that stabilizing noncovalent interactions leads to less total hsA-coordinated Ru(III) species after long incubation times.

In previous studies of the bis-indazole (KP1019) and bis-imidazole (KP418) Keppler-type complexes (Figure 1), we have observed significant differences in noncovalent interactions with hsA.[21] KP1019 forms noncovalent interactions with hsA very rapidly, which prevents precipitation, and has been linked to the low level of side effects observed in clinical

dx.doi.org/10.1021/ic202029e | *Inorg. Chem.* 2012, 51, 954–966

studies.[5,6,21] As with NAMI-A, noncovalently hsA-bound KP1019 complexes are slowly converted to protein coordinated species. By contrast, KP418 does not form noncovalent interactions with hsA, demonstrating that the imidazole ligands are less favorable toward these types of interactions.[21] Interestingly, the aquated derivatives of KP418 do form noncovalent interactions with hsA, and these interactions are sufficiently favored that they prevent covalent binding to the protein. This demonstrates that noncovalent interactions with hsA are influenced not only by the potential of the axial ligands to interact directly with the protein, but also by the charge and perhaps polarity of the complexes.

Effect of Protein Binding on Reductive Stability. The "activation by reduction" hypothesis for Ru(III) anticancer compounds postulates that conversion to Ru(II) species in vivo by biological reducing agents activates them toward ligand substitution and increases their propensity for binding to biomolecules.[64] In the case of DNA interactions, this process can then lead to apoptosis.[1] This has been proposed as a targeting strategy for these compounds, since they could be preferentially reduced in the hypoxic environments frequently found in tumors.[64] Intracellular processes may not be as relevant to the activity of NAMI-A-type complexes as they are to Keppler-type complexes. However, modulation of the oxidation state in blood after intravenous infusion is anticipated to be important to mediate interactions with many extracellular biomolecule targets, and is likely an important component of antimetastatic activity.[3,10,24,65]

The cyclic voltammograms of compounds **1a,b**, **2a,b**, and **3a,b** were measured in physiological buffer with a Ag/AgCl working electrode and scan rates of 100 mV/s (Supporting Information, Figures S34–S39). Because of the lower solubility of compounds **4a** and **4b**, they were dissolved in a 1:1 mixture of DMSO and buffer, before measurement of their cyclic voltammograms (Supporting Information, Figures S40, S41). To determine the effect of DMSO on the reduction potentials, the cyclic voltammograms of NAMI-A were measured in both buffer (Supporting Information, Figure S42) and 1:1 DMSO/physiological buffer (Supporting Information, Figure S43). These measurements indicate a shift in electrochemical potential to lower values (ca. 160 mV).

For each complex a one-electron Ru(III) → Ru(II) redox couple was observed. As shown in Table 2, the values of $E_{1/2}$ for **1a,b**–**3a,b** are very similar, as expected given the similar donating properties of the pyridine ligands, and fall in the range of 320–340 mV. Addition of the solvent correction for **4a** and **4b** gives 320 and 330 mV, respectively. These values are all slightly higher than previous electrochemical measurements which report $E_{1/2}$ for **1b** in aqueous solution of 300 mV[30] and for **2a** in buffered saline (pH 7.40),[50] of 310 mV vs NHE in each case,[66] likely reflecting minor differences in the experimental methods used.

Table 2. Reduction Potentials of Compounds 1a,b–4a,b vs NHE[a]

LH^+ counterion	**1a**	**2a**	**3a**	**4a**
$E_{1/2}$ Ru(III/II) (mV)	330 (80)	320 (70)	330 (120)	160 (100)[b]
Na^+ counterion	**1b**	**2b**	**3b**	**4b**
$E_{1/2}$ Ru(III/II) (mV)	330 (70)	320 (70)	330 (80)	170 (90)[b]

[a]Peak-to-peak differences in parentheses ($|E_{pc} - E_{pa}|$) (mV). [b]Compounds **4a** and **4b** measured in 1:1 DMSO/buffer. See main text for solvent-correction to $E_{1/2}$.

As pointed out in previous reports,[42,64] the reduction potentials of these types of ruthenium complexes can be estimated using the additive description of ligand contributions to $E_{1/2}$ given by Lever's equation (eq 1).[67]

$$E = S_M \sum E_L + I_M \quad (1)$$

The electrochemical ligand parameter, E_L, correlates with the net electron donating character of the constituent ligands of redox-active metal complexes. S_M and I_M are paramaters derived from the empirical correspondence between $\sum E_L$, and experimental values of $E_{1/2}$ for a particular redox couple. The reduction potential has been shown to be dependent on solvent environment and the overall charge of the complexes measured.[67] Reisner et al. have reported values of S_M = 0.88 and I_M = 0.46 for Ru(III)(−1) → Ru(II)(−2) in neutral phosphate buffer solutions.[64] Ligand parameters of $E_L(Cl^-)$ = −0.24,[67] E_L(DMSO, S-coordinated) = 0.57,[68] E_L(Pyr) = 0.25,[67] and E_L(mePyr) = 0.23[67] give, from eq 1, $E_{1/2}$(**1a,b**) = 330 mV and $E_{1/2}$(**2a,b**) = 320 mV, in good agreement with our experimental values (Table 2). Values of E_L for NbenzPyr and dibenzPyr have not been reported previously, but the experimental values of $E_{1/2}$ found here indicate they are very similar to Pyr and mePyr, with $E_L \approx 0.25$.

The values of $E_{1/2}$ for the pyridine analogues described here are significantly more positive than NAMI-A, which has previously been reported as $E_{1/2}$ = 260 mV versus NHE in a 0.10 M phosphate buffer system at pH 7.4,[69,70] and is found to be $E_{1/2}$ = 270 mV under the aqueous buffer conditions used in this work. The higher reduction potentials of **1a,b**–**4a,b** reflect the greater net electron donating character of pyridine as compared to imidazole (E_L(imidazole) = 0.09[71]). These reduction potentials are readily accessible to biological reducing agents such as ascorbic acid ($E°$ = +60 mV vs NHE) and glutathione ($E°$ = −250 mV vs NHE).[64] Several earlier studies have shown that the Ru(III) center of NAMI-A is reduced readily to Ru(II) in the presence of ascorbic acid.[16,17,60] EPR measurements can be used to follow this process by tracking the overall loss of signal intensity because of the production of diamagnetic Ru(II) centers from paramagnetic Ru(III) species. To study the reduction behavior of the pyridine complexes described here, we initially incubated each compound with an equimolar concentration of ascorbic acid in buffer at 37 °C. For each complex, **1a,b**–**4a,b**, this leads to essentially complete loss of the EPR signal after less than 10 min of incubation (data not shown), demonstrating that reduction of almost all Ru(III) centers occurs very rapidly, as expected given the relatively high reduction potential of these compounds.

To determine the influence of protein interactions on the reduction of the Ru(III) centers of **1a,b**–**4a,b** the complexes were first incubated with hsA and the resulting solutions were then mixed with buffered ascorbic acid solutions, to give solutions with 1:1 molar ratios of ruthenium complexes/ascorbic acid. In the first of these experiments, protein-bound fractions of each complex were prepared by briefly mixing each complex with hsA in buffer at 25 °C, followed by ultrafiltration. These solutions were then combined with buffered ascorbic acid and briefly mixed at 25 °C. As described in the previous section, this initial incubation procedure with hsA produces significant concentrations of noncovalently bound complexes for **1a,b**–**4a,b**, as shown by distinctive EPR signals (Figure 5

dx.doi.org/10.1021/ic202029e | Inorg. Chem. 2012, 51, 954–966

and Supporting Information, Figures S13−S20). However, as shown by the EPR spectra labeled "0 min" in Figure 7 and

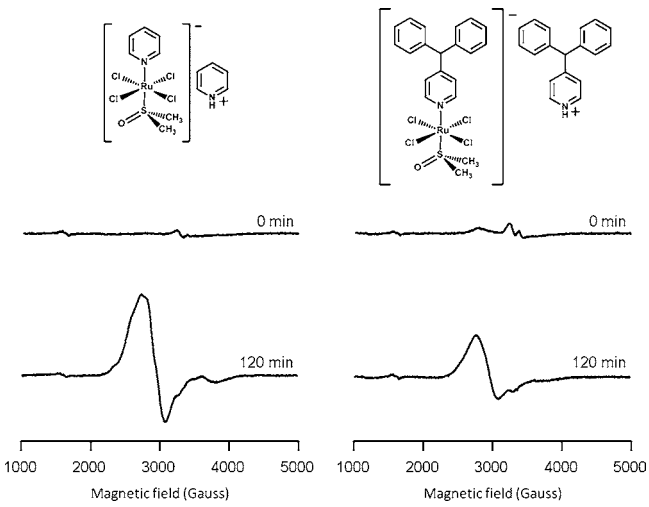

Figure 7. EPR measurement of **1a** and **4a** after initial incubation with hsA in physiological buffer at 37 °C for the times shown; followed by addition of ascorbic acid. **Experimental parameters:** frequency = 9.38 GHz, microwave power = 2.0 mW, time constant = 40.96 ms, modulation amplitude = 6 G, average of five 2-min scans. For EPR spectra of analogous experiments with other complexes see Supporting Information, Figure S21.

Supporting Information, Figure S21a, the addition of ascorbic acid reduces these species to give EPR-silent Ru(II) centers, demonstrating that noncovalent binding to the hydrophobic binding domains of hsA does not limit interactions with exogenous reducing agents.

Incubation of **1a,b**−**4a,b** with hsA for 120 min at 37 °C, gives, almost exclusively, complexes that are covalently protein bound, as described above, with corresponding EPR spectra (Figure 5 and Supporting Information, Figures S13−S20). In contrast to the noncovalently bound species, addition of ascorbic acid causes no change to the appearance or intensity of the EPR spectra from these species (Figure 7 and Supporting Information, Figure S21b). This indicates that covalent binding to hsA prevents reduction and thus can give mononuclear Ru(III) species in vivo. This increase in the reductive stability can be explained by the effect of ligand exchange on $E_{1/2}$. Since the complexes are expected to be bound primarily to surface imidazoles of hsA histidine residues, the effect of covalent binding on the reduction potential can be estimated from eq 1 using the value of the ligand parameter for imidazole. Histidine imidazole (His-Im) coordination at the axial position, initially occupied by DMSO (species **1a**-hsA-2 in Figure 5 and corresponding species in Supporting Information, Figures S13−S20 for other complexes) gives [*trans*-$RuCl_4$(1*H*-L)(His-Im)]$^-$. Assuming that this Ru(III) species can be described with a −1 charge, and correspondingly S_M = 0.88 and I_M = 0.46, then eq 1 gives $E_{1/2}$ = −0.90 mV, which is sufficiently negative to prevent reduction by ascorbic acid. Substitution of a Cl^- ligand for a histidine imidazole gives $RuCl_3$(His-Im)(1*H*-L)(DMSO-*S*). This neutral complex is then described by eq 1 with S_M = 0.97 and I_M = 0.04,[64] which gives $E_{1/2}$ = 220 mV, and thus this species is predicted to be readily reduced by ascorbic acid. However, if the lower-symmetry hsA-coordinated species (such as **1a**-hsA-1 in Figure 5) has histidine imidazole coordination at an equatorial position, and undergoes DMSO exchange with water ($E_L(H_2O)$ = 0.04), to give the neutral species $RuCl_3$(His-Im)(1*H*-L)(H_2O), then eq 1 gives $E_{1/2}$ = −390 mV, and so this species is expected to be resistant to reduction by ascorbic acid. This scenario seems reasonable, given the demonstrated proclivity of these complexes to undergo DMSO exchange. Although there is some uncertainty in these calculations for a variety of reasons, they do demonstrate the overall concept that a combination of ligand exchange with H_2O and protein side chains can produce species that are resistant to reduction under physiological conditions.

Similar enhancement in reductive stability with protein binding has also been reported for NAMI-A,[17] and this has been suggested as a method for targeted activation of these types of compounds.[64] Lowering of the reduction potential by protein binding allows for transport in vivo in the Ru(III) oxidation state without reduction by physiological reducing agents. However, the reduction potential found in proliferating cells ($E_{1/2} \approx -240$ mV[72]), can be reduced by as much as 100 mV in hypoxic tumor environments.[73] This provides the potential for reduction of Ru(III) species that would otherwise be redox stabilized under physiological conditions.[69] The production of more labile Ru(II) species then facilitates coordination to biomolecules and apoptosis.[1,64]

CONCLUSIONS

It is now widely accepted that protein interactions are a key component of the pro-drug behavior of anticancer Ru(III) complexes. Binding to hsA is expected to be predominant in vivo and is thus central to the transport and speciation of these compounds. As we have shown here using pyridine complexes, the properties of the axial azole ligand of NAMI-A-like complexes play a critical role in modulating interactions with hsA. From EPR studies we have demonstrated that the rates of ligand exchange in buffer solution are relatively unaffected by the characteristics of the pyridine ligands. However, these ligands do control the persistence of noncovalent protein interactions, through distinct abilities to interact with the hydrophobic binding domains of hsA. This not only controls speciation, as compared to buffer solution, but also affects the concentration of covalently bound mononuclear Ru(III) species after long incubation periods. As we have shown, noncovalently bound complexes are readily reduced by ascorbic acid, while covalently bound complexes are not. Consequently, it seems likely that increased stability of noncovalent interactions reduces the concentration of Ru(III) species found in vivo. Overall, these results indicate that tuning noncovalent interactions of Ru(III) complexes with hsA through the selection of suitable axial azole ligands is an important component of their activity and selectivity, and should be considered as part of future drug design strategies.

ASSOCIATED CONTENT

Supporting Information

For compounds **1a,b**−**4a,b**: (i) EPR spectra, and spectral deconvolutions by simulation, for all incubation times, up to 2 h with buffer, hsA, hsA and ascorbic acid; (ii) tables of *g* values and line widths for EPR spectral simulations; (iii) NMR spectra; (iv) crystallographic data in CIF format and tables of Ru-ligand bond lengths for each compounds except **4a**; (v) cyclic voltammogram traces. This material is available free of charge via the Internet at http://pubs.acs.org.

dx.doi.org/10.1021/ic202029e | *Inorg. Chem.* 2012, 51, 954−966

AUTHOR INFORMATION

Corresponding Author

*E-mail: cwalsby@sfu.ca.

ACKNOWLEDGMENTS

The authors are grateful to Prof. Tim Storr for assistance with the electrochemical measurements, and Dr. Michael Katz for assistance with X-ray structures of **1b** and **2b**. Financial support was provided by The Natural Sciences and Engineering Research Council of Canada (NSERC), The Canada Foundation for Innovation (CFI), and Simon Fraser University.

REFERENCES

(1) Clarke, M. J. *Coord. Chem. Rev.* **2002**, *232*, 69−93.
(2) Jakupec, M. A.; Galanski, M.; Arion, V. B.; Hartinger, C. G.; Keppler, B. K. *Dalton Trans.* **2008**, 183−194. Dyson, P. J.; Sava, G. *Dalton Trans.* **2006**, 1929−1933. de Paula, Q. A.; Franco, R. W. D.; Ribeiro, M. B.; Ellena, J.; Castellano, E. E.; Nascimento, O. R.; Batista, A. A. *J. Mol. Struct.* **2008**, *891*, 64−74. Kennedy, D. C.; Patrick, B. O.; James, B. R. *Can. J. Chem.* **2011**, *89*, 948−958.
(3) Levina, A.; Mitra, A.; Lay, P. A. *Metallomics* **2009**, *1*, 458−470.
(4) Rademaker-Lakhai, J. M.; van den Bongard, D.; Pluim, D.; Beijnen, J. H.; Schellens, J. H. M. *Clin. Cancer Res.* **2004**, *10*, 3717−3727. Lentz, F.; Drescher, A.; Lindauer, A.; Henke, M.; Hilger, R. A.; Hartinger, C. G.; Scheulen, M. E.; Dittrich, C.; Keppler, B. K.; Jaehde, U. *Anti-Cancer Drugs* **2009**, *20*, 97−103.
(5) Hartinger, C. G.; Zorbas-Seifried, S.; Jakupec, M. A.; Kynast, B.; Zorbas, H.; Keppler, B. K. *J. Inorg. Biochem.* **2006**, *100*, 891−904.
(6) Hartinger, C. G.; Jakupec, M. A.; Zorbas-Seifried, S.; Groessl, M.; Egger, A.; Berger, W.; Zorbas, H.; Dyson, P. J.; Keppler, B. K. *Chem. Biodiversity* **2008**, *5*, 2140−2155.
(7) Mestroni, G.; Alessio, E.; Sava, G.; Pacor, S.; Coluccia, M.; Boccarelli, A. *Met.-Based Drugs* **1994**, *1*, 41−63.
(8) Sava, G.; Capozzi, I.; Clerici, K.; Gagliardi, G.; Alessio, E.; Mestroni, G. *Clin. Exp. Metastasis* **1998**, *16*, 371−379.
(9) Bacac, M.; Vadori, M.; Sava, G.; Pacor, S. *Cancer Immunol. Immunother.* **2004**, *53*, 1101−1110. Bergamo, A.; Cocchietto, M.; Capozzi, I.; Mestroni, G.; Alessio, E.; Sava, G. *Anti-Cancer Drugs* **1996**, *7*, 697−702. Cocchietto, M.; Zorzet, S.; Sorc, A.; Sava, G. *Invest. New Drugs* **2003**, *21*, 55−62. Frausin, F.; Scarcia, V.; Cocchietto, M.; Furlani, A.; Serli, B.; Alessio, E.; Sava, G. *J. Pharmacol. Exp. Ther.* **2005**, *313*, 227−233. Pacor, S.; Zorzet, S.; Cocchietto, M.; Bacac, M.; Vadori, M.; Turrin, C.; Gava, B.; Castellarin, A.; Sava, G. *J. Pharmacol. Exp. Ther.* **2004**, *310*, 737−744. Pintus, G.; Tadolini, B.; Posadino, A. M.; Sanna, B.; Debidda, M.; Bennardini, F.; Sava, G.; Ventura, C. *Eur. J. Biochem.* **2002**, *269*, 5861−5870. Sava, G.; Alessio, E.; Bergamo, A.; Mestroni, G. *Top. Biol. Inorg. Chem.* **1999**, *1*, 143−169. Sava, G.; Clerici, K.; Capozzi, I.; Cocchietto, M.; Gagliardi, R.; Alessio, E.; Mestroni, G.; Perbellini, A. *Anti-Cancer Drugs* **1999**, *10*, 129−138. Zorzet, S.; Bergamo, A.; Cocchietto, M.; Sorc, A.; Gava, B.; Alessio, E.; Iengo, E.; Sava, G. *J. Pharmacol. Exp. Ther.* **2000**, *295*, 927−933. Zorzet, S.; Sorc, A.; Casarsa, C.; Cocchietto, M.; Sava, G. *Met.-Based Drugs* **2001**, *8*, 1−7.
(10) Bergamo, A.; Sava, G. *Dalton Trans.* **2007**, 1267−1272. Gava, B.; Zorzet, S.; Spessotto, P.; Cocchietto, M.; Sava, G. *J. Pharmacol. Exp. Ther.* **2006**, *317*, 284−291. Sava, G.; Zorzet, S.; Turrin, C.; Vita, F.; Soranzo, M.; Zabucchi, G.; Cocchietto, M.; Bergamo, A.; DiGiovine, S.; Pezzoni, G.; Sartor, L.; Garbisa, S. *Clin. Cancer Res.* **2003**, *9*, 1898−1905.
(11) Kreuser, E. D.; Keppler, B. K.; Berdel, W. E.; Piest, A.; Thiel, E. *Semin. Oncol.* **1992**, *19*, 73−81.
(12) Cebrian-Losantos, B.; Reisner, E.; Kowol, C. R.; Roller, A.; Shova, S.; Arion, V. B.; Keppler, B. K. *Inorg. Chem.* **2008**, *47*, 6513−6523.
(13) Keppler, B. K.; Rupp, W.; Juhl, U. M.; Endres, H.; Niebl, R.; Balzer, W. *Inorg. Chem.* **1987**, *26*, 4366−4370.
(14) Alessio, E.; Mestroni, G.; Bergamo, A.; Sava, G. *Curr. Top. Med. Chem.* **2004**, *4*, 1525−1535.
(15) Bacac, M.; Hotze, A. C. G.; van der Schilden, K.; Haasnoot, J. G.; Pacor, S.; Alessio, E.; Sava, G.; Reedijk, J. *J. Inorg. Biochem.* **2004**, *98*, 402−412.
(16) Sava, G.; Bergamo, A.; Zorzet, S.; Gava, B.; Casarsa, C.; Cocchietto, M.; Furlani, A.; Scarcia, V.; Serli, B.; Iengo, E.; Alessio, E.; Mestroni, G. *Eur. J. Cancer* **2002**, *38*, 427−435.
(17) Webb, M. I.; Walsby, C. J. *Dalton Trans.* **2011**, *40*, 1322−1331.
(18) Lipponer, K.-G.; Vogel, E.; Keppler, B. K. *Met.-Based Drugs* **1996**, *3*, 243−260.
(19) Pieper, T.; Peti, W.; Keppler, B. K. *Met.-Based Drugs* **2000**, *7*, 225−232.
(20) Ni Dhubhghaill, O. M.; Hagen, W. R.; Keppler, B. K.; Lipponer, K.-G.; Sadler, P. J. *J. Chem. Soc., Dalton Trans.* **1994**, 3305−3310. Chatlas, J.; van Eldik, R.; Keppler, B. K. *Inorg. Chim. Acta* **1995**, *233*, 59−63.
(21) Cetinbas, N.; Webb, M. I.; Dubland, J. A.; Walsby, C. J. *J. Biol. Inorg. Chem.* **2010**, *15*, 131−145.
(22) Kratz, F. *Metal Complexes in Cancer Chemotherapy*; VCH: Weinheim, Germany, 1993; pp 391−429. Timerbaev, A. R.; Hartinger, C. G.; Aleksenko, S. S.; Keppler, B. K. *Chem. Rev.* **2006**, *106*, 2224−2248.
(23) Kratz, F.; Mulinacci, N.; Messori, L.; Bertini, I.; Keppler, B. K. In *Proceedings of the 2nd International Symposium on Metal Ions in Biology and Medicine*John Libbey EurotextParis, France; 1992; pp 69−74
(24) Liu, M. M.; Lim, Z. J.; Gwee, Y. Y.; Levina, A.; Lay, P. A. *Angew. Chem., Int. Ed.* **2010**, *49*, 1661−1664.
(25) Messori, L.; Vilchez, F. G.; Vilaplana, R.; Piccioli, F.; Alessio, E.; Keppler, B. *Met.-Based Drugs* **2000**, *7*, 335−342.
(26) Bergamo, A.; Messori, L.; Piccioli, F.; Cocchietto, M.; Sava, G. *Invest. New Drugs* **2003**, *21*, 401−411.
(27) Sava, G.; Pacor, S.; Mestroni, G.; Alessio, E. *Clin. Exp. Metastasis* **1992**, *10*, 273−280.
(28) Heffeter, P.; Bock, K.; Atil, B.; Hoda, M. A. R.; Korner, W.; Bartel, C.; Jungwirth, U.; Keppler, B. K.; Micksche, M.; Berger, W.; Koellensperger, G. *J. Biol. Inorg. Chem.* **2010**, *15*, 737−748. Polec-Pawlak, K.; Abramski, J. K.; Ferenc, J.; Foteeva, L. S.; Timerbaev, A. R.; Keppler, B. K.; Jarosz, M. *J. Chromatogr., A* **2008**, *1192*, 323−326.
(29) Alessio, E.; Balducci, G.; Calligaris, M.; Costa, G.; Attia, W. M.; Mestroni, G. *Inorg. Chem.* **1991**, *30*, 609−618.
(30) Alessio, E.; Balducci, G.; Lutman, A.; Mestroni, G.; Calligaris, M.; Attia, W. M. *Inorg. Chim. Acta* **1993**, *203*, 205−217.
(31) Betteridge, P. W.; Carruthers, J. R.; Cooper, R. I.; Prout, K.; Watkin, D. J. *J. Appl. Crystallogr.* **2003**, *36*, 1487.
(32) Farrugia, L. J. *J. Appl. Crystallogr.* **1997**, *30*, 565.
(33) *Persistence of Vision Raytracer*, 3.6.1; Persistence of Vision Pty. Ltd: Williamstown, Victoria, Australia, 2004.
(34) Stoll, S.; Schweiger, A. *J. Magn. Reson.* **2006**, *178*, 42−55.
(35) Mestroni, G.; Alessio, E.; Sava, G. New salts of anionic complexes of Ru(III), as antimetastatic and antineoplastic agents; European Patent: 3401 9800431; 6 June, 1997.
(36) Mestroni, G.; Alessio, E.; Sava, G. New salts of anionic complexes of Ru(III), as antimetastatic and antineoplastic agents; 1997-EP3401 9800431; 19970630., 1998; Mestroni, G.; Alessio, E.; Sava, G. Salts of anionic complexes of Ru(III), as antimetastatic and antineoplastic agents; U.S. Patent 6,221,905; 24 April, 2001.
(37) Kljun, J.; Petricek, S.; Zigon, D.; Hudej, R.; Miklavcic, D.; Turel, I. *Bioinorg. Chem. Appl.* **2010**, DOI: DOI: 10.1155/2010/183097.
(38) Liang, Y. H.; Liang, G. G. *Chin. J. Inorg. Chem.* **2008**, *24*, 1983−1988.
(39) Mura, P.; Camalli, M.; Messori, L.; Piccioli, F.; Zanello, P.; Corsini, M. *Inorg. Chem.* **2004**, *43*, 3863−3870.
(40) Velders, A. H.; Bergamo, A.; Alessio, E.; Zangrando, E.; Haasnoot, J. G.; Casarsa, C.; Cocchietto, M.; Zorzet, S.; Sava, G. *J. Med. Chem.* **2004**, *47*, 1110−1121.
(41) Groessl, M.; Reisner, E.; Hartinger, C. G.; Eichinger, R.; Semenova, O.; Timerbaev, A. R.; Jakupec, M. A.; Arion, V. B.; Keppler, B. K. *J. Med. Chem.* **2007**, *50*, 2185−2193.

(42) Reisner, E.; Arion, V. B.; Fatima, M.; da Silva, C. G.; Lichtenecker, R.; Eichinger, A.; Keppler, B. K.; Kukushkin, V. Y.; Pombeiro, A. J. L. *Inorg. Chem.* **2004**, *43*, 7083−7093.
(43) Reisner, E.; Arion, V. B.; Eichinger, A.; Kandler, N.; Giester, G.; Pombeiro, A. J. L.; Keppler, B. K. *Inorg. Chem.* **2005**, *44*, 6704−6716.
(44) Ravera, M.; Gabano, E.; Baracco, S.; Sardi, M.; Osella, D. *Inorg. Chim. Acta* **2008**, *361*, 2879−2886.
(45) Griffith, D.; Ceeco, S.; Zangrando, E.; Bergamo, A.; Sava, G.; Marmion, C. J. *J. Biol. Inorg. Chem.* **2008**, *13*, 511−520.
(46) de Paula, Q. A.; Batista, A. A.; Nascimento, O. R.; da Costa, A. J.; Schultz, M. S.; Bonfadini, M. R.; Oliva, G. *J. Braz. Chem. Soc.* **2000**, *11*, 530−536.
(47) Geremia, S.; Alessio, E.; Todone, F. *Inorg. Chim. Acta* **1996**, *253*, 87−90.
(48) Sava, G.; Pacor, S.; Bergamo, A.; Cocchietto, M.; Mestroni, G.; Alessio, E. *Chem. Biol. Interact.* **1995**, *95*, 109−126.
(49) Alberti, F. M.; Fiol, J. J.; Garcia-Raso, A.; Torres, M.; Terron, A.; Barcelo-Oliver, M.; Prieto, M. J.; Moreno, V.; Molins, E. *Polyhedron* **2010**, *29*, 34−41.
(50) Liang, Y. H.; Bi, W.; Liang, G. G. *Chin. J. Inorg. Chem.* **2011**, *27*, 595−603.
(51) Travnicek, Z.; Matikova-Malarova, M.; Novotna, R.; Vanco, J.; Stepankova, K.; Suchy, P. *J. Inorg. Biochem.* **2011**, *105*, 937−948. Anderson, C. M.; Herman, A.; Rochon, F. D. *Polyhedron* **2007**, *26*, 3661−3668.
(52) Delferro, M.; Marchio, L.; Tegoni, M.; Tardito, S.; Franchi-Gazzola, R.; Lanfranchi, M. *Dalton Trans.* **2009**, 3766−3773.
(53) Seddon, E. A.; Seddon, K. R. *The Chemistry of Ruthenium*; Elsevier Science Publishing Co. Inc.: Amsterdam, The Netherlands, 1984.
(54) Anderson, C.; Beauchamp, A. L. *Can. J. Chem.* **1995**, *73*, 471−482.
(55) Quinlan, G. J.; Martin, G. S.; Evans, T. W. *Hepatology* **2005**, *41*, 1211−1219. Fischer, M. J. E.; Bos, O. J. M.; van der Linden, R. F.; Wilting, J.; Janssen, L. H. M. *Biochem. Pharmacol.* **1993**, *45*, 2411−2416. Pedersen, S. M. *Biochem. Pharmacol.* **1987**, *36*, 2661−2666. Sudlow, G.; Birkett, D. J.; Wade, D. N. *Mol. Pharmacol.* **1975**, *11*, 824−32. Sudlow, G.; Birkett, D. J.; Wade, D. N. *Mol. Pharmacol.* **1976**, *12*, 1052−61. Zunszain, P. A.; Ghuman, J.; Komatsu, T.; Tsuchida, E.; Curry, S. *BMC Struct. Biol.* **2003**, *3*, 6.
(56) Peters, T. *Adv. Protein Chem.* **1985**, *37*, 161−245.
(57) Groessl, M.; Hartinger, C. G.; Egger, A.; Keppler, B. K. *Met. Ions Biol. Med.* **2006**, *9*, 111−116.
(58) Trynda-Lemiesz, L.; Karaczyn, A.; Keppler, B. K.; Kozlowski, H. *J. Inorg. Biochem.* **2000**, *78*, 341−346. Trynda-Lemiesz, L.; Luczkowski, M. *Bioinorg. Chem. Appl.* **2003**, 141−150.
(59) Messori, L.; Orioli, P.; Vullo, D.; Alessio, E.; Iengo, E. *Eur. J. Biochem.* **2000**, *267*, 1206−1213.
(60) Brindell, M.; Stawoska, I.; Supel, J.; Skoczowski, A.; Stochel, G.; van Eldik, R. *J. Biol. Inorg. Chem.* **2008**, *13*, 909−918.
(61) Hnizda, A.; Santrucek, J.; Sanda, M.; Strohalm, M.; Kodicek, M. *J. Biochem. Biophys. Methods* **2008**, *70*, 1091−1097.
(62) Ivanov, A. I.; Christodoulou, J.; Parkinson, J. A.; Barnham, K. J.; Tucker, A.; Woodrow, J.; Sadler, P. J. *J. Biol. Chem.* **1998**, *273*, 14721−14730.
(63) Kragh-Hansen, U.; Chuang, V. T. G.; Otagiri, M. *Biol. Pharm. Bull.* **2002**, *25*, 695−704.
(64) Reisner, E.; Arion, V. B.; Keppler, B. K.; Pombeiro, A. J. L. *Inorg. Chim. Acta* **2008**, *361*, 1569−1583.
(65) Sava, G.; Frausin, F.; Cocchietto, M.; Vita, F.; Podda, E.; Spessotto, P.; Furlani, A.; Scarcia, V.; Zabucchi, G. *Eur. J. Cancer* **2004**, *40*, 1383−1396.
(66) Original measurement of electrochemical potential for **1b** vs SSCE, $E_{1/2}$ vs NHE calculated by adding 236 mV; **2a** vs SCE, $E_{1/2}$ vs NHE calculated by adding 241 mV.
(67) Lever, A. B. P. *Inorg. Chem.* **1990**, *29*, 1271−1285.
(68) Guedes da Silva, M. F. C.; Pombeiro, A. J. L.; Geremia, S.; Zangrando, E.; Calligaris, M.; Zinchenko, A. V.; Kukushkin, V. Y. *J. Chem. Soc., Dalton Trans.* **2000**, 1363−1371.
(69) Ravera, M.; Baracco, S.; Cassino, C.; Zanello, P.; Osella, D. *Dalton Trans.* **2004**, 2347−2351.
(70) Original measurement of electrochemical potential for NAMI-A vs SCE, $E_{1/2}$ vs NHE calculated by adding 241 mV.
(71) Clarke, M. J.; Bailey, V.; Doan, P.; Hiller, C.; LaChance-Galang, K. J.; Daghlian, H.; Mandal, S.; Bastos, C. M.; Lang, D. *Inorg. Chem.* **1996**, *35*, 4896−4903.
(72) Schafer, F. Q.; Buettner, G. R. *Free Radical Biol. Med.* **2001**, *30*, 1191−1212.
(73) Miklavcic, D.; Sersa, G.; Novakovic, S.; Rebersek, S. *J. Bioelectr.* **1990**, *9*, 133−149.